

Weakly-Supervised Attention and Relation Learning for Facial Action Unit Detection

Zhiwen Shao, Zhilei Liu, Jianfei Cai, *Senior Member, IEEE*, Yunsheng Wu, and Lizhuang Ma

Abstract—Attention mechanism has recently attracted increasing attentions in the field of facial action unit (AU) detection. By finding the region of interest (ROI) of each AU with the attention mechanism, AU related local features can be captured. Most existing AU detection works design fixed attentions based on the prior knowledge, without considering the nonrigidity of AUs and relations among AUs. In this paper, we propose a novel end-to-end weakly-supervised attention and relation learning framework for AU detection, which has not been explored before. In particular, to select and extract AU related features, both channel-wise attentions and spatial attentions are learned with AU labels only. Moreover, pixel-level relations for AUs are learned to refine spatial attentions and extract more accurate local features. A multi-scale local region learning method is further proposed to adapt multi-scale AUs in different locations, which can facilitate the weakly-supervised attention and relation learning. Extensive experiments on BP4D and DISFA benchmarks demonstrate that our framework (i) outperforms the state-of-the-art methods for AU detection, and (ii) also achieves superior performance of AU intensity estimation with a simple extension.

Index Terms—Weakly-supervised, attention learning, relation learning, facial AU detection, multi-scale local region learning

1 INTRODUCTION

FAcial action unit (AU) detection is an important face analysis task. It recognizes facial expressions by analyzing cues of some atomic muscle movements in local facial regions. A very comprehensive set of facial atomic muscle movements, namely action units (AUs), is defined by Facial Action Coding System (FACS) [1]. Attention mechanism has been adopted in various structural prediction tasks such as saliency detection [2], object recognition [3], and image captioning [4], where great success has been achieved. By finding the region of interest (ROI) of each AU with the attention mechanism, more accurate features can be captured. However, in literature only a few works proposed attention based methods, in which prior knowledge is required to predefine the attentions of AUs.

Facial landmarks have been used for defining the attentions to provide rough locations of AUs [5], [6], [7], since facial AU detection is related to facial landmark detection [8]. Li et al. [5], [6] proposed a deep learning based method using predefined attentions for AU detection, in which landmarks are used to generate the ROI with a fixed size and a fixed attention distribution for each AU. Sanchez et al. [7] utilized an hourglass network [9] for AU intensity estimation by regressing from the input image to attention

maps, where the ground-truth attention maps are defined by landmarks and AU intensities with a Gaussian distribution. These methods design fixed attentions based on the prior knowledge about the location relationship between AUs and landmarks, which are handcrafted and have limited capacity to model various AUs with non-rigid muscle movements. The implicit attentions adaptively learned with the supervision from AU detection should be utilized to extract AU related local features. However, in literature it is rare to see methods with adaptively learned attentions for AU detection.

In this paper, we propose a novel deep learning based weakly-supervised attention and relation learning (WSARL) framework for AU detection. Our method learns the implicit attentions and relations in a weakly-supervised manner with AU labels only. Different from other tasks like object recognition [3], there is no distinct contour and texture for AUs, making weakly-supervised attention and relation learning of AUs a more challenging problem. In order to learn attentions with respect to each AU respectively, each AU has an independent branch of attention and relation learning. First, to select and extract features, both channel-wise attention learning and spatial attention learning are used. Since a channel of a feature map is the result of a certain filter, channel-wise attention learning can be seen as the process of feature selection. Spatial attention learning is further used to find the ROI of each AU and extract accurate local features. Second, to exploit the relations among AUs in different local facial regions, we use Conditional Random Fields as Recurrent Neural Networks (CRF-RNN) [10] for pixel-level relation learning. With the captured relations among AUs, spatial pixel-wise attentions of each AU are refined and more related local features can be extracted. Third, we propose a multi-scale local region learning method since well-learned features are important for challenging weakly-supervised attention and relation learning. The learned

- Z. Shao is with the Department of Computer Science and Engineering, Shanghai Jiao Tong University, Shanghai 200240, China. E-mail: shaozhiwen@sjtu.edu.cn.
- Z. Liu is with the School of Computer Science and Technology, Tianjin University, Tianjin 300072, China. E-mail: zhileiliu@tju.edu.cn.
- J. Cai is with the School of Computer Science and Engineering, Nanyang Technological University, 50 Nanyang Ave, Singapore 639798. E-mail: asjfc@ntu.edu.sg.
- Y. Wu is with the Tencent YouTu, Shanghai 200233, China. E-mail: simonwu@tencent.com.
- L. Ma is with the School of Computer Science and Software Engineering, East China Normal University, Shanghai 200062, China, and the Department of Computer Science and Engineering, Shanghai Jiao Tong University, Shanghai 200240, China. E-mail: ma-lz@cs.sjtu.edu.cn.

multi-scale features are shared for all the AUs. Specifically, Feature maps are partitioned into multi-scale local regions, each of which is processed with an independent filter, for adapting multi-scale AUs in different locations. The entire framework is end-to-end for joint learning of attention and relation, without any post-processing step.

The contributions of this paper are summarized below.

- A weakly-supervised attention learning method is proposed for AU detection. We show that our proposed channel-wise attention learning and spatial attention learning both contribute to AU detection. To the best of our knowledge, weakly-supervised channel-wise and spatial attention learning with AU labels only has not been done before.
- Pixel-level relation learning for each AU is proposed to capture the relations among AUs and refine spatial attentions. It is demonstrated that three types of relations among AUs including close relations, slight relations, and no relation are all captured by our proposed pixel-level relation learning.
- A multi-scale local region learning method is proposed to adapt multi-scale AUs in different locations. It is shown that the learned multi-scale features facilitate the weakly-supervised attention and relation learning, and improve the AU detection performance with a large margin.
- Extensive experiments demonstrate that our framework WSARL outperforms the state-of-the-art methods including both traditional methods and deep learning based methods for AU detection, and also achieves superior performance of AU intensity estimation with a simple extension.

2 RELATED WORK

Facial AU detection has been studied extensively over the past decades, however as mentioned before, the attention mechanism was used by only a few recent works. Here we will first review the attention based facial AU detection methods. Existing relation based and region learning based facial AU detection methods will also be reviewed, since our framework uses the pixel-level relation learning and multi-scale local region learning.

2.1 Attention Based Facial AU Detection

It is hard to annotate the attentions of each AU manually, since AUs have no distinct contour and texture and may change across persons and facial expressions. For this challenging attention learning of AUs, a few recent methods use facial landmarks to define the attentions of each AU based on prior knowledge. Li et al. [5] proposed an Enhancing and Cropping Net (EAC-Net) for AU detection by using predefined attentions to enhance and crop the ROIs of AUs. The ROI of each AU has a fixed size and a fixed attention distribution, whose location is given by landmarks. R-T1 [6] improves the EAC-Net by using Long Short Term Memory (LSTM) [11] to fuse temporal features of a sequence of images. Sanchez et al. [7] employed an hourglass network [9] for attention map regression to estimate all AU intensities. Similarly, the ground-truth attention map of each AU is

predefined with a Gaussian distribution, where landmarks determine the center and AU intensities determine the amplitude and size.

All these methods demonstrate the effectiveness of attention mechanism for AU detection. However, they all design fixed attentions based on the prior knowledge, without refining the attentions adaptively during the training process.

2.2 Relation Based Facial AU Detection

AU detection is a multi-label classification problem, where the relations among AUs can be exploited to improve the performance of each AU. Zhang et al. [12] proposed a multi-task multiple kernel learning method to learn a kernel representation which encodes the AU relations. Zhao et al. [13] proposed a Joint Patch and Multi-Label Learning (JPML) framework for AU detection by modeling the joint dependence behind features, AUs, and their interplay. Two AU relations, positive correlation and negative competition, are computed by statistically analyzing the training datasets. Wu et al. [8] utilized a cascade regression framework to capture global AU relations and global dependencies between AUs and landmarks. Eleftheriadis et al. [14] proposed a multi-conditional latent variable model to jointly detect multiple AUs based on handcrafted features, in which both local and global dependencies among AUs are encoded.

In contrast with these methods, we employ an end-to-end deep learning framework to model the pixel-level relations for each AU. The relation learning is integrated with the attention learning to capture more accurate relations among AUs.

2.3 Region Learning Based Facial AU Detection

Different AUs occur in different facial local regions, thus region learning based AU detection has attracted increasing attention recently. Liu et al. [15] partition a face image into uniform patches to extract local features, which are further disentangled into common features and expression-specific features. JPML [13] uses group sparsity learning to select patches for each AU, where the patches are centered around the landmarks. Inspired by the locally connected layer [16], Zhao et al. [17] proposed a region layer to process each uniformly partitioned patch with independent convolutional filters. EAC-Net [5] crops the ROI of each AU to extract AU related local features. Corneanu et al. [18] combined patch learning and structure learning, where five patches around points of interest are cropped.

These methods all use the patches with identical sizes, which limits their performance for multi-scale AUs. In contrast, we propose the multi-scale local region learning to extract local features from multi-scale patches.

3 WSARL FOR FACIAL AU DETECTION

3.1 Overview

Our proposed framework WSARL is shown in Fig. 1, including two modules, multi-scale local region learning, and attention and relation learning. In particular, the multi-scale local region learning extracts features of multi-scale local regions as the foundation of our framework. The learned features are further utilized to facilitate the weakly-supervised

attention and relation learning of each AU. Moreover, the attention and relation learning is designed as the central role for AU detection, which learns the attentions and relations adaptively for each AU with an independent branch respectively. The channel-wise attention learning selects features, and the spatial attention learning with pixel-level relation learning further extracts AU related local features.

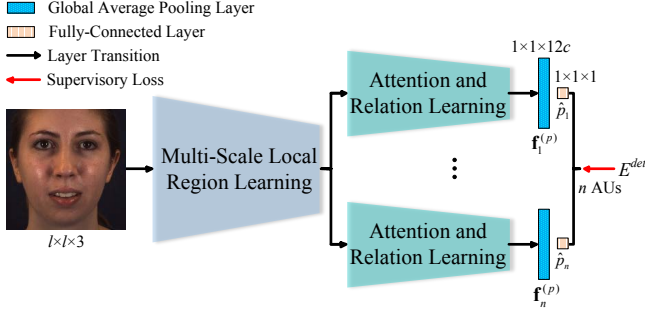


Fig. 1. Architecture of the proposed WSARL framework. Each AU has the same structure of attention and relation learning.

As illustrated in Fig. 1, the input of our framework is a color face image with the size of $l \times l \times 3$. After the attention and relation learning, for the i -th AU, the learned AU related feature is finally processed to be a feature $\mathbf{f}_i^{(p)} \in \mathbb{R}^{12c \times 1}$ using the Global Average Pooling layer [19]. The estimated occurrence probability is computed with a sigmoid function $\sigma(\cdot)$ formulated as

$$\hat{p}_i = \sigma(\mathbf{w}_i^{(p)T} \mathbf{f}_i^{(p)}), \quad i = 1, \dots, n, \quad (1)$$

where $\mathbf{w}_i^{(p)} \in \mathbb{R}^{12c \times 1}$ denotes the weight parameters of the final one-dimensional fully-connected layer, and n is the number of AUs. Without loss of generality, we simplify the notation of linear mapping $\mathbf{w}_i^{(p)T} \mathbf{f}_i^{(p)}$ by omitting the bias term.

Most of the AU detection benchmarks suffer from the imbalance of occurrence rates of AUs [20], which is harmful to training. Considering AU detection is a multi-label binary classification problem, to alleviate the data imbalance issue, we use weighted sigmoid cross entropy loss for AU detection formulated as

$$E^{det} = \sum_{i=1}^n w_i [p_i \log \hat{p}_i + (1 - p_i) \log(1 - \hat{p}_i)], \quad (2)$$

where p_i denotes the ground-truth occurrence probability of the i -th AU, and w_i denotes the weight of the loss of the i -th AU. Specifically, we set

$$w_i = \frac{1/r_i}{\sum_{i=1}^n (1/r_i)}, \quad (3)$$

where r_i is the occurrence rate of the i -th AU of the training set.

3.2 Multi-Scale Local Region Learning

Most deep learning based methods [21], [22] utilize plain convolutional layers to learn features, in which convolutional filter weights are shared across an entire feature map. Considering that different AUs occur in different local

facial regions, Zhao et al. [17] proposed a region layer with independent convolutional filters for each of 8×8 local patches. However, the proposed region layer partitions the feature map into patches with identical sizes, which can not adapt multi-scale AUs. In this paper, we propose the multi-scale local region learning to process multi-scale local patches with independent filters.

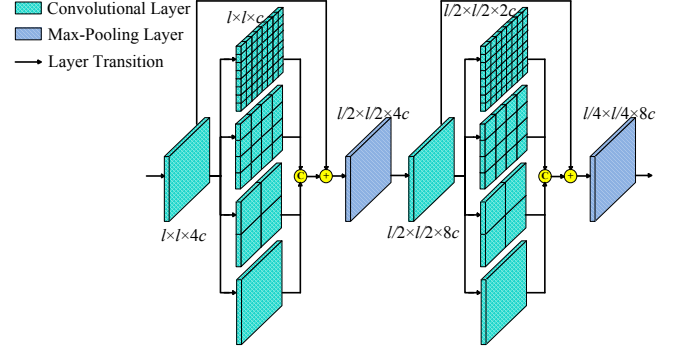


Fig. 2. Architecture of the module of multi-scale local region learning, where $l \times l \times c$ indicates that the height, width, and channel of the corresponding layer are l , l , and c respectively, and “C” and “+” denote concatenation and element-wise sum respectively.

Fig. 2 shows the architecture of the module of multi-scale local region learning. It consists of two blocks of multi-scale local region learning, each of which is followed by a max-pooling layer over 2×2 spatial fields with a stride 2. A block of multi-scale local region learning contains an input convolutional layer and four intermediate convolutional layers, each of which use 3×3 convolution filters with a stride 1 and a padding 1. The feature map of the input layer is followed by Batch Normalization (BN) [23] and Rectified Linear Unit (ReLU) [24] and is partitioned into 8×8 , 4×4 , 2×2 , and 1×1 patches respectively, which are fed into the four intermediate layers respectively. The feature maps of the four intermediate layers are first concatenated to integrate the extracted multi-scale local features, and are further summed element-wisely with the feature map of the input layer, finally followed by BN and ReLU. Note that the element-wise sum operation is used as a residual structure [25] which is beneficial for avoiding the vanishing gradient problem. Our proposed module of multi-scale local region learning extracts rich local features which contribute to further attention and relation learning of each AU.

3.3 Attention Learning

Our proposed attention learning method learns both channel-wise attentions and spatial attentions. Fig. 3 illustrates the structure of attention and relation learning of a certain AU. For the i -th AU, we apply a convolution operation to the output of the module of multi-scale local region learning and obtain a feature $\mathbf{f}_i^{(1)}$. Then we use a Global Average Pooling layer for $\mathbf{f}_i^{(1)}$ and obtain the channel-wise feature $\mathbf{f}_i^{(1c)} \in \mathbb{R}^{12c \times 1}$. The channel-wise attention weights $\mathbf{v}_i^{(c)} \in \mathbb{R}^{12c \times 1}$ are computed as

$$\mathbf{v}_i^{(c)} = \sigma(\mathbf{W}_i^{(1c)T} \mathbf{f}_i^{(1c)}), \quad i = 1, \dots, n, \quad (4)$$

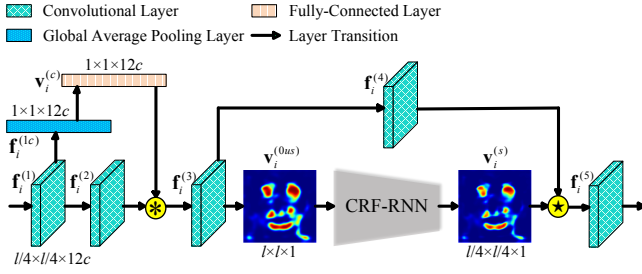


Fig. 3. Structure of attention and relation learning of a certain AU, where all the convolutional layers have the same size of $l/4 \times l/4 \times 12c$, and “*” and “ \star ” denote channel-wise multiplication and element-wise multiplication, respectively. Spatial attentions of an example AU 7 are shown, where the regions of eyes, cheeks, lips, and lip corners are highlighted. After using CRF-RNN [10], spatial attentions are refined to be smoother with small isolated regions removed.

where $\mathbf{W}_i^{(1c)} \in \mathbb{R}^{12c \times 12c}$ denotes the weight parameters of the $12c$ -dimensional fully-connected layer, and $\sigma(\cdot)$ is operated on each element of the vector. Meanwhile, a feature $\mathbf{f}_i^{(2)}$ is generated using a convolution operation on the feature $\mathbf{f}_i^{(1)}$. We obtain the channel-wise weighted feature defined as

$$\mathbf{f}_i^{(c)} = \mathbf{v}_i^{(c)} * \mathbf{f}_i^{(2)}, \quad i = 1, \dots, n, \quad (5)$$

where $*$ denotes the channel-wise multiplication of feature map channels and corresponding channel weights. It is shown that each convolutional filter performs as a pattern detector [26]. Since a channel of a feature map is the response of a certain filter, our proposed channel-wise attention learning is beneficial for selecting related attributes.

During the process of spatial attention learning, a feature $\mathbf{f}_i^{(3)}$ is first generated by applying a convolution operation to the feature $\mathbf{f}_i^{(c)}$. Then we use a convolutional layer with one channel for $\mathbf{f}_i^{(3)}$ and obtain spatial feature $\mathbf{f}_i^{(3s)}$ with the size of $l/4 \times l/4 \times 1$. To be consistent with the input face image, $\mathbf{f}_i^{(3s)}$ is upsampled to be a new feature $\mathbf{f}_i^{(3us)}$ with the size of $l \times l \times 1$ using bilinear interpolation [27]. The initial spatial attention weights are formulated as

$$\mathbf{v}_i^{(0us)} = \sigma(\mathbf{f}_i^{(3us)}), \quad i = 1, \dots, n, \quad (6)$$

where $\mathbf{v}_i^{(0us)} = (v_{i1}^{(0us)}, \dots, v_{im}^{(0us)})$, $m = l \times l$ is the number of pixels of the input image, and $\sigma(\cdot)$ is operated on each element of $\mathbf{f}_i^{(3us)}$.

3.4 Relation Learning

We use CRF-RNN [10] to model spatial pixel-level relations for each AU, which is beneficial for refining the spatial attentions, respectively. Learning spatial attentions is a pixel-wise binary classification problem. Denote $y_{ij} \in \{0, 1\}$ as the attention label of the j -th pixel for the i -th AU, where $j = 1, \dots, m$. In the fully connected CRF-RNN model, the energy of a label assignment $\mathbf{y}_i = (y_{i1}, \dots, y_{im})$ is defined as

$$E_i^{crf}(\mathbf{y}_i) = \sum_j \psi_i^u(y_{ij}) + \sum_{j < k} \psi_i^p(y_{ij}, y_{ik}), \quad i = 1, \dots, n, \quad (7)$$

where $\psi_i^u(y_{ij}) = -\log P^{(0)}(y_{ij})$ is the unary potential which measures the cost of assigning label y_{ij} to the j -th

pixel, $P^{(0)}(y_{ij})$ is the initial label assignment probability of the j -th pixel, and $\psi_i^p(y_{ij}, y_{ik})$ is the pairwise potential. Note that $P^{(0)}(y_{ij}) = P^{(0)}(y_{ij} = 1) = v_{ij}^{(0us)}$ if $v_{ij}^{(0us)} \geq 0.5$, and otherwise $P^{(0)}(y_{ij}) = P^{(0)}(y_{ij} = 0) = 1 - v_{ij}^{(0us)}$. The pairwise potential is modeled with weighted Gaussian kernels as

$$\psi_i^p(y_{ij}, y_{ik}) = \mu_i(y_{ij}, y_{ik}) [w_i^{(1)} \exp(-\frac{\|\mathbf{p}_j - \mathbf{p}_k\|^2}{2\alpha_i^2} - \frac{\|\mathbf{I}_j - \mathbf{I}_k\|^2}{2\beta_i^2}) + w_i^{(2)} \exp(-\frac{\|\mathbf{p}_j - \mathbf{p}_k\|^2}{2\gamma_i^2})], \quad (8)$$

where $\mu_i(\cdot, \cdot)$ is the label compatibility function, \mathbf{p}_j and \mathbf{I}_j denote the position vector and RGB color vector of the j -th pixel of the input face image, the hyperparameters $w_i^{(1)}$ and $w_i^{(2)}$ control the relative importance of two Gaussian kernels, and the hyperparameters α_i , β_i , and γ_i control the scale of Gaussian kernels. The first kernel enforces nearby pixels with similar color to have the same label, and the second kernel is used for enforcing smoothness. We use the mean-field approximation method proposed by [10] to learn refined label assignment probability, denoted as $P(y_{ij})$. The refined spatial attention weight at each pixel is defined as

$$v_{ij}^{(us)} = P(y_{ij} = 1). \quad (9)$$

In particular, the refined spatial attention weights of the i -th AU are $\mathbf{v}_i^{(us)} = (v_{i1}^{(us)}, \dots, v_{im}^{(us)})$. $\mathbf{v}_i^{(us)}$ is further downsampled to be $\mathbf{v}_i^{(s)}$ with the size of $l/4 \times l/4 \times 1$ using bilinear interpolation.

After applying a convolutional layer for $\mathbf{f}_i^{(3)}$, a feature $\mathbf{f}_i^{(4)}$ is learned. The spatial weighted feature is defined as

$$\mathbf{f}_i^{(s)} = \mathbf{v}_i^{(s)} \star \mathbf{f}_i^{(4)}, \quad i = 1, \dots, n, \quad (10)$$

where \star denotes the element-wise multiplication of each feature map channel and the spatial attention weights. According to Fig. 3 and Fig. 1, the finally learned AU related feature $\mathbf{f}_i^{(p)}$ is extracted by processing $\mathbf{f}_i^{(s)}$ with a convolutional layer and a Global Average Pooling layer. With the CRF-RNN, our proposed relation learning method exploits the relations between each pair of pixels to refine spatial pixel-wise attentions. In the module of attention and relation learning, $\mathbf{f}_i^{(1)}$, $\mathbf{f}_i^{(c)}$, $\mathbf{f}_i^{(3)}$, and $\mathbf{f}_i^{(s)}$ are followed by BN and ReLU.

As illustrated in Fig. 3, small isolated regions are removed in the refined spatial attentions, which is beneficial for extracting AU related local features. Moreover, the spatial attentions of AU 7 are highlighted in eyes, cheeks, lips, and lip corners, which correspond to the ROI of AU 7, AU 6, AU 10, and AU 12 respectively according to the prior knowledge. It is shown that AU 7 and AU 6, AU 7 and AU 10, AU 7 and AU 12 have positive correlations [13]. Therefore, the learned spatial attentions of a certain AU are highlighted in the ROIs of both current AU and a few other closely related AUs. Note that the attentions in the ROI of current AU have higher and wider responses than other regions. Our proposed attention and relation learning can both find the ROIs of AUs and capture the relations among AUs in a weakly-supervised manner.

TABLE 1

F1-frame and accuracy for 12 AUs on BP4D. Best results are shown in bold and brackets. Second best results are shown in bold. Note that only the F1-Frame results are reported by DSIN [18].

AU	F1-Frame						Accuracy				
	LSVM	JPML	DRML	EAC-Net	DSIN	WSARL	LSVM	JPML	DRML	EAC-Net	WSARL
1	23.2	32.6	36.4	39.0	[51.7]	50.4	20.7	40.7	55.7	68.9	[76.2]
2	22.8	25.6	[41.8]	35.2	40.4	35.1	17.7	42.1	54.5	[73.9]	[73.9]
4	23.1	37.4	43.0	48.6	[56.0]	51.1	22.9	46.2	58.8	[78.1]	76.7
6	27.2	42.3	55.0	[76.1]	[76.1]	74.4	20.3	40.0	56.6	[78.5]	76.6
7	47.1	50.5	67.0	72.9	73.5	[77.1]	44.8	50.0	61.0	69.0	[73.4]
10	77.2	72.2	66.3	[81.9]	79.9	81.6	73.4	75.2	53.6	77.6	[77.8]
12	63.7	74.1	65.8	86.2	85.4	[86.9]	55.3	60.5	60.8	84.6	[85.2]
14	64.3	[65.7]	54.1	58.8	62.7	57.8	46.8	53.6	57.0	[60.6]	60.5
15	18.4	38.1	33.2	37.5	37.3	[48.9]	18.3	50.1	56.2	78.1	[82.8]
17	33.0	40.0	48.0	59.1	[62.9]	58.8	36.4	42.5	50.0	[70.6]	69.3
23	19.4	30.4	31.7	35.9	38.8	[48.7]	19.2	51.9	53.9	81.0	[81.2]
24	20.7	42.3	30.0	35.8	41.6	[54.2]	11.7	53.2	53.9	82.4	[84.8]
Avg	35.3	45.9	48.3	55.9	58.9	[60.4]	32.2	50.5	56.0	75.2	[76.5]

We incorporate the two losses E^{det} and E_i^{crf} from Eqs. 2 and 7, which yields the complete loss for AU detection

$$E = E^{det} + \sum_{i=1}^n E_i^{crf}. \quad (11)$$

Our proposed framework is trainable end-to-end, where attentions and relations are learned with the supervision from AU detection and the mean-field approximation of CRF-RNN.

4 EXPERIMENTS

4.1 Datasets and Settings

4.1.1 Datasets

Our method WSARL is evaluated on two popular datasets BP4D [28] and DISFA [29] for facial AU detection. Each dataset is coded with FACS [1] by certified experts. Note that the CK+ [30] dataset is not used because only video-level annotations are given, while we aim at frame-level prediction.

- **BP4D** contains 23 female and 18 male participants associating with 8 sessions, i.e. 328 videos in total. These videos are both 2D and 3D, including about 140,000 frames coded with AU occurrence. Similar to the settings in previous works [5], [17], we perform subject exclusive 3-fold cross-validation with the same subject partition rule on 12 AUs.
- **DISFA** contains 27 participants with 12 females and 15 males, each of which was recorded by a video with 4,845 frames. Each frame was labeled with AU intensities from 0 to 5. Following the settings of [5], [17], the AU intensity equal or greater than 2 is considered as occurrence, otherwise considered as absence. Our network is initialized with the BP4D trained model and further retrained for 8 AUs using subject exclusive 3-fold cross-validation.

4.1.2 Implementation Details

Each face image is aligned to be $200 \times 200 \times 3$ using similarity transformation including rotation, uniform scaling, and translation, whose shape is preserved without facial expression changes. Before inputted to our framework, each

face is randomly cropped into $176 \times 176 \times 3$ and maybe further horizontally flipped. The parameter l is thus 176, and the parameter c is chosen to be 8. Our framework is trained for up to 12 epochs using Caffe [31] with stochastic gradient descent (SGD), a mini-batch size of 8, a weight decay of 0.0005, and a momentum of 0.9. The learning rate starts with 0.006 and is multiplied by a factor of 0.3 at every 2 epochs. The pixel-level relation learning with CRF-RNN for each AU uses 10 mean-field iterations, and the hyperparameters $w_i^{(1)}$, $w_i^{(2)}$, α_i , β_i , and γ_i are obtained by cross validation on a small set of training data.

4.1.3 Evaluation Metrics

We use two metrics, frame-based F1-score (F1-frame) and accuracy, to measure the performance of AU detection for comparisons with the literature. For a binary classification problem, F1-frame can better evaluate the method especially when samples are imbalanced [14]. F1-frame is formulated as

$$F1 = \frac{2PR}{P + R}, \quad (12)$$

where P and R denote precision and recall respectively. The average results over all AUs (Avg) are also reported. In the following sections, % is omitted in the results of F1-frame and accuracy.

4.2 Comparison with State-of-the-Art Methods

We compare our method WSARL against state-of-the-art methods under the same 3-fold cross validation setting. These methods include both traditional methods, LSVM [32], APL [33], and JPML [13], and deep learning based methods, DRML [17], EAC-Net [5], and DSIN [18]. For fairness, we use the results of LSVM, APL, and JPML reported in [5], [17]. Note that several methods like CNN+LSTM [34], R-T1 [6] are not compared, since they process a sequence of images instead of a single image.

4.2.1 Evaluation on BP4D

Table 1 reports the F1-frame and accuracy results of our method WSARL and state-of-the-art methods on BP4D. It can be observed that our proposed WSARL outperforms all the state-of-the-art methods on the challenging BP4D benchmark, especially for traditional methods including LSVM

TABLE 2

F1-frame and accuracy for 8 AUs on DISFA. Best results are shown in bold and brackets. Second best results are shown in bold. Note that only the F1-Frame results are reported by DSIN [18].

AU	F1-Frame						Accuracy				
	LSVM	APL	DRML	EAC-Net	DSIN	WSARL	LSVM	APL	DRML	EAC-Net	WSARL
1	10.8	11.4	17.3	41.5	42.4	[51.0]	21.6	32.7	53.3	85.6	[93.0]
2	10.0	12.0	17.7	26.4	[39.0]	32.3	15.8	27.8	53.2	84.9	[92.0]
4	21.8	30.1	37.4	66.4	[68.4]	61.3	17.2	37.9	60.0	79.1	[83.8]
6	15.7	12.4	29.0	[50.7]	28.6	40.3	8.7	13.6	54.9	69.1	[90.7]
9	11.5	10.1	10.7	[80.5]	46.8	47.6	15.0	64.4	51.5	88.1	[96.4]
12	70.4	65.9	37.7	[89.3]	70.8	74.5	93.8	[94.2]	54.6	90.0	93.2
25	12.0	21.4	38.5	88.9	90.4	[94.0]	3.4	50.4	45.6	80.5	[96.6]
26	22.1	26.9	20.1	15.6	42.2	[56.8]	20.1	47.1	45.3	64.8	[89.2]
Avg	21.8	23.8	26.7	48.5	53.6	[57.2]	27.5	46.0	52.3	80.6	[91.9]

and APL. DSIN [18] is a most recent work showing significant performance, which is also based on deep learning and models relations among AUs like our WSARL. Compared to the state-of-the-art DSIN, WSARL further advances the average F1-frame of AU detection to a higher level 60. Besides highest results of average F1-frame and average accuracy, WSARL exhibits competitive performance for each AU compared with other methods.

There are a few interesting observations about EAC-Net, which is a typical attention based AU detection method. For AU 10 and AU 12 with discriminative texture, EAC-Net reveals advantages and outperforms DSIN. In contrast to EAC-Net with fixed attentions, our method WSARL reaches the same level of performance using adaptively learned attentions. For less discriminative AUs, WSARL significantly outperforms EAC-Net, which demonstrates the effectiveness of our proposed weakly-supervised attention and relation learning.

4.2.2 Evaluation on DISFA

The F1-frame and accuracy results evaluated on DISFA benchmark are shown in Table 2, where it can be seen that our WSARL significantly outperforms all the previous works with even larger margins. In particular, WSARL brings relative increments of 6.72% for average F1-frame over DSIN and 14.02% for average accuracy over EAC-Net. Note that there is a severer data imbalance problem [5] in DISFA than BP4D, which causes major fluctuations in performances of different AUs of most previous methods especially for LSVM and APL. Due to the effectiveness of weakly-supervised attention and relation learning and weighted loss in Eq. 2, WSARL achieves high and stable performance for each AU. Moreover, as illustrated in Table 1 and Table 2, WSARL is superior to the traditional methods LSVM, APL, and JPML, which demonstrates the strength of deep learning based methods.

4.3 Ablation Study

In this section, we perform experiments to evaluate the effectiveness of each component in our framework. Table 3 summarizes the structures and F1-frame results of different variants of our proposed WSARL. B-Net is a baseline network with plain convolutional layers, pooling layers, and fully-connected layers, whose corresponding parts are replaced with the proposed components for different variants.

4.3.1 Attention Learning

S-Net learns spatial attentions of each AU and increase the average F1-frame to 56.2 over B-Net. Note that the effectiveness of spatial attention learning requires the facilitating from multi-scale local region learning and relation learning. There are implicit attention mechanisms in deep neural networks [17]. Our proposed spatial attention learning method learns spatial attentions and weights features, which explicitly represents the feature learning process of the deep neural network. By learning spatial attentions, even if multi-scale local region learning and relation learning are not used, S-Net advances the average F1-frame from level 55 to the level 56. After representing the channel-wise attention mechanism of the deep neural network explicitly, SC-Net further improves the AU detection performance. Similar to spatial attention learning, the integration with relation learning and multi-scale local region learning can contribute to the effectiveness of channel-wise attention learning.

4.3.2 Multi-Scale Local Region Learning

SCR-Net uses the region learning method proposed by [17], which is treated as an another baseline network. By processing each local face region with independent filters, SCR-Net increases the average F1-frame with a large margin 1.7 over SC-Net. SCM-Net uses our proposed multi-scale local region learning by considering multi-scale local face regions, and further improves the AU detection performance with the average F1-frame of 59.0. The significant margin 2.4 between the results of SCM-Net and SC-Net demonstrates that multi-scale local region learning can extract useful features to facilitate spatial attention learning and channel-wise attention learning. Note that a block of multi-scale local region learning has fewer parameters than a block of region learning [17]. This is because that the four intermediate convolutional layers of multi-scale local region learning have fewer filters than the intermediate layer of region learning. Therefore our proposed multi-scale local region learning has stronger capacity of feature learning than region learning with fewer parameters.

4.3.3 Relation Learning

Base on the structure of SCM-Net, our WSARL further uses pixel-level relation learning to refine learned spatial attentions of each AU. By exploiting the relations between each pair of pixels, WSARL achieves significant performance with the average F1-frame of 60.4. Pixel-level relation

TABLE 3

F1-frame for 12AUs of different variants of our proposed WSARL on BP4D. **SA**: Spatial attention. **CA**: Channel-wise attention. **R**: Region learning [17]. **MR**: Multi-scale local region learning. **PR**: Pixel-level relation learning. Best results are shown in bold and brackets. Second best results are shown in bold.

Method	SA	CA	R	MR	PR	1	2	4	6	7	10	12	14	15	17	23	24	Avg
B-Net						42.0	30.5	49.4	70.5	74.3	79.3	81.7	55.7	33.5	55.7	44.6	49.5	55.6
S-Net	✓					45.1	30.4	46.3	72.2	74.6	76.9	84.7	53.7	42.8	58.3	40.9	48.2	56.2
SC-Net	✓	✓				40.4	30.4	47.7	70.5	75.4	80.2	83.3	[58.5]	44.6	57.4	43.3	47.3	56.6
SCR-Net	✓	✓	✓			43.9	35.5	46.7	72.2	76.3	80.9	86.4	58.3	44.8	[61.3]	46.3	47.2	58.3
SCM-Net	✓	✓		✓		49.2	[38.9]	49.2	71.2	75.5	80.3	86.6	55.3	48.3	58.7	45.0	49.9	59.0
WSARL	✓	✓		✓	✓	[50.4]	35.1	[51.1]	[74.4]	[77.1]	[81.6]	[86.9]	57.8	[48.9]	58.8	[48.7]	[54.2]	[60.4]

learning plays an important role in the learning of spatial attentions, in which the implicit relations among AUs are utilized. As mentioned before, the significant performance of our framework is attributed to the integration of attention learning, relation learning, and multi-scale local region learning.

4.4 Qualitative Results

4.4.1 Channel-Wise Attention Learning

It is indicated that each convolutional filter performs as a pattern detector [26]. Take AU 24 of BP4D benchmark as an example, several channels of $f_i^{(2)}$ with superior attention weights are visualized in Fig. 4. To observe the pattern detected by the corresponding filter of each channel, visualized results are overlaid on the input image. We can observe that different filters emphasize on different facial attributes. In particular, the first channel emphasizes on the regions of brow and above the brow, which are related to many AUs such as AU 1 and AU 2. The second channel detects distinctive facial regions including the eyes, nose, and ears. The third and the fourth emphasize on lower parts and upper parts of a face respectively, and the fifth detects remaining facial regions including the distinctive mouth. Therefore our proposed channel-wise attention learning can select features generated by the filters which detect the patterns related to AU detection. Note that the features selected by our proposed channel-wise attention learning are rich, which will be further processed to be related to the corresponding AU by spatial attention learning and pixel-level relation learning.

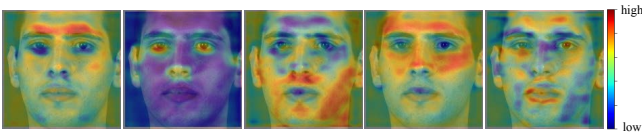


Fig. 4. Visualization of several attentive channels of $f_i^{(2)}$ for AU 24. Colors on each channel indicate different values from low to high, as shown in the color bar.

4.4.2 Pixel-Level Relation Learning for Refining Spatial Attention

To investigate the effect of our proposed pixel-level relation learning on spatial attentions, we visualize the initial spatial attention weights $v_i^{(0us)}$ and refined spatial attention weights $v_i^{(s)}$ for several AUs of an example image in Fig. 5. It is seen that refined spatial attentions are smoother with

small isolated regions removed. Specifically, take AU 2 as an example, the noisy attentions in the regions of cheeks, profiles, and mouth are significantly reduced, and the correct attentions in the region of brow are preserved. Moreover, the useless attentions in the background are removed, as shown in the AU 2, AU 15, and AU 24. It can be concluded that our proposed pixel-level relation learning is beneficial for capturing more accurate attentions and extracting more related local features.

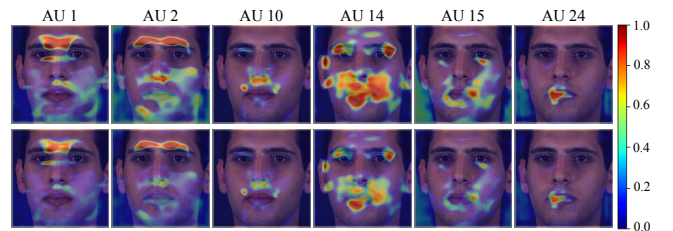


Fig. 5. Visualization of initial spatial attention weights $v_i^{(0us)}$ and refined spatial attention weights $v_i^{(s)}$ of an example image from BP4D. The first and the second row show $v_i^{(0us)}$ and $v_i^{(s)}$, respectively. Attention weights are visualized with the colors shown in the color bar.

4.4.3 WSARL

Here we illustrate that our proposed framework WSARL can find the ROIs of AUs and capture the relations among AUs. In particular, we visualize the spatial attention weights $v_i^{(s)}$ of WSARL and predefined spatial attention weights of EAC-Net [5] for all the 12 AUs of example images from BP4D in Fig. 6. There are several interesting observations from the visualization results as follows:

- The ROI of each AU has an attention distribution which may change across persons and facial expressions. From the learned spatial attention weights of WSARL for the first image and the second image, it is observed that the ROIs of the same AU from the same expression of different persons have different attentions. On the other hand, by comparing the results of the second image with the third image, it is observed that the ROIs of the same AU from different expressions of the same person also have different attentions. In contrast to our WSARL, EAC-Net uses landmarks to generate the ROI with a fixed attention distribution for each AU, which can not adapt diverse expressions and non-rigid AUs.
- The ROI of each AU has an irregular boundary which is difficult to be determined by prior knowledge.

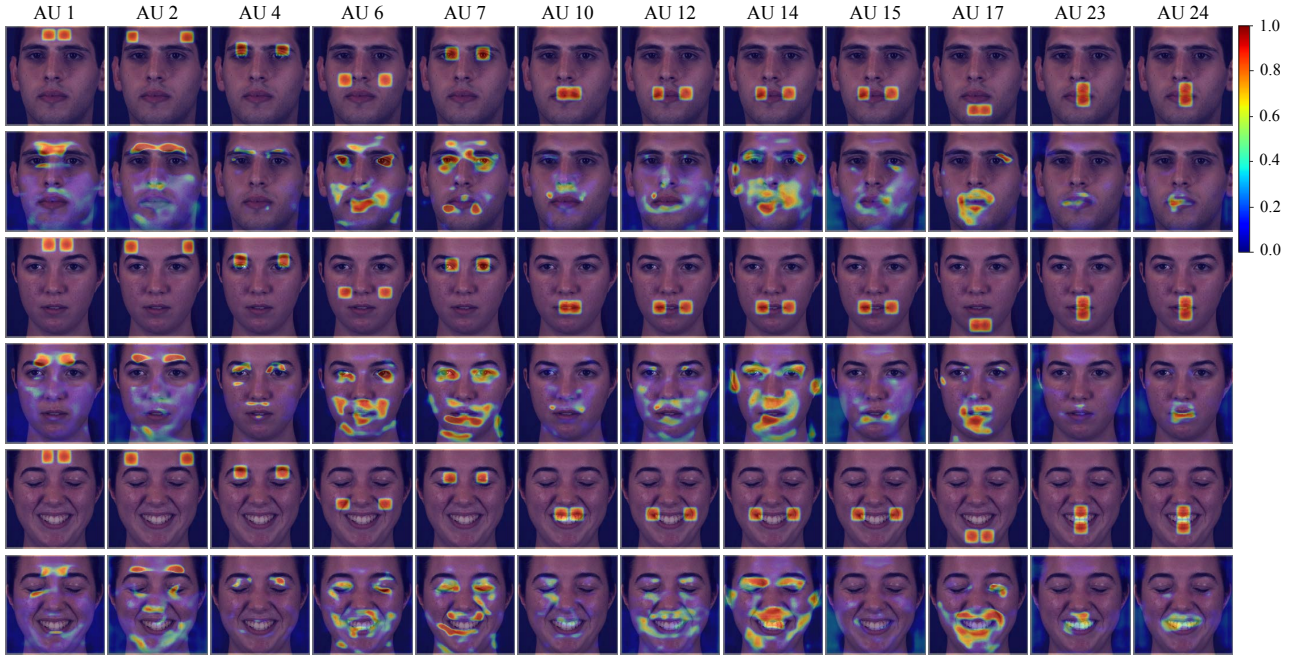


Fig. 6. Visualization of spatial attention weights of 12 AUs for three BP4D images. The first image and the second image have a same facial expression, and the second and the third are from a same person with different expressions. The first, third, and fifth rows show the predefined spatial attention weights of EAC-Net [5], and the second, fourth, and sixth rows show the learned spatial attention weights $\mathbf{v}_i^{(s)}$ of our method WSARL. Attention weights are visualized with the colors shown in the color bar.

A fixed size and a square boundary used by EAC-Net for ROIs have limited capacity to model various AUs. By learning the ROIs of AUs adaptively, our WSARL can extract accurate AU related local features. Note that our learned spatial attentions are approximately highlighted in predefined ROIs of EAC-Net, which demonstrates the effectiveness of our proposed WSARL.

- Highlighted attentions occur in the ROIs of both current AU and a few other closely related AUs. Some examples about our learned spatial attentions are analyzed below. First, the attentions of AU 1 and AU 2 are both highlighted above the brow, and AU 6 and AU 7 have similar attentions, which demonstrate the close relations between AU 1 and AU 2, and between AU 6 and AU 7. Second, the attentions of AU 7 have small responses in the ROI of AU 10, and the attentions of AU 6 have small responses in the ROI of AU 23, which demonstrates the slight relations between AU 7 and AU 10, and between AU 6 and AU 23. Third, according to the learned attentions, AU 4 has no relation to AU 15, AU 17, AU 23, and AU 24. Therefore our proposed pixel-level relation learning captures three types of relations among AUs including close relations, slight relations, and no relation.

In addition, there is no distinct contour and texture for some AUs, whose centers of ROIs are difficult to be determined accurately by landmarks. Note that EAC-Net do not define the location relationship between landmarks and AU 9, AU 25, and AU 26 of DISFA benchmark. We show the visualized spatial attention weights $\mathbf{v}_i^{(s)}$ of our WSARL for the three AUs in Fig. 7. It is observed that our method

WSARL can adaptively learn spatial attentions for various expressions from different persons. Moreover, WSARL is robust to illumination variations and occlusions.



Fig. 7. Visualization of spatial attention weights $\mathbf{v}_i^{(s)}$ of our method WSARL for AU 9, AU 25, and AU 26 of DISFA benchmark. The second image and the fifth image are in a different illumination environment from other images, and the fifth image is occluded by eyeglasses. Attention weights are visualized with the colors shown in the color bar.

4.5 WSARL for AU Intensity Estimation

Facial AU intensity estimation is closely related to facial AU detection, where the intensities from 0 to 5 of AUs are required to be recognized. To evaluate the effectiveness for AU intensity estimation, our framework is performed with a simple extension. Specifically, the outputs of our framework are first computed by Eq. 1 and further multiplied by 5 to obtain the predicted intensities \hat{p}_i^{int} . We use a weighted Euclidean loss for AU intensity estimation defined as

$$E^{int} = \frac{1}{2} \sum_{i=1}^n w_i (p_i^{int} - \hat{p}_i^{int})^2, \quad (13)$$

TABLE 4

ICC and MAE for 5 AUs on FERA 2015. Best results are shown in bold and brackets. Second best results are shown in bold. Note that only the ICC results are reported by MRF, LT-all, and COR-HIT.

AU	ICC							MAE			
	MRF	LT-all	COR-HIT	DRML	OR-CNN	CCNN-IT	i-WSARL	DRML	OR-CNN	CCNN-IT	i-WSARL
6	0.72	0.69	[0.76]	0.62	0.60	0.75	0.73	1.37	1.37	1.14	[0.66]
10	0.71	0.58	0.72	0.64	0.61	0.69	[0.74]	1.25	1.39	1.30	[0.76]
12	0.81	0.76	0.81	0.74	0.59	[0.86]	[0.86]	1.13	1.37	0.99	[0.56]
14	0.33	0.30	0.29	0.31	0.25	0.40	[0.44]	1.59	1.80	1.65	[1.07]
17	0.30	0.31	0.36	0.32	0.31	0.45	[0.52]	1.16	1.19	1.08	[0.75]
Avg	0.58	0.53	0.59	0.52	0.47	0.63	[0.66]	1.30	1.42	1.23	[0.76]

TABLE 5

ICC and MAE for 12 AUs on DISFA. Best results are shown in bold and brackets. Second best results are shown in bold.

AU	ICC				MAE			
	DRML	OR-CNN	CCNN-IT	i-WSARL	DRML	OR-CNN	CCNN-IT	i-WSARL
1	0.05	0.03	0.18	[0.41]	0.85	1.05	0.87	[0.33]
2	0.06	0.07	0.15	[0.42]	0.70	0.87	0.63	[0.55]
4	0.32	0.01	[0.61]	0.55	1.07	1.47	[0.86]	0.92
5	0.02	0.00	0.07	[0.48]	0.20	[0.17]	0.26	0.18
6	0.36	0.29	[0.65]	0.59	0.75	0.79	0.73	[0.46]
9	0.39	0.08	[0.55]	0.24	0.58	0.70	0.57	[0.43]
12	0.77	0.67	[0.82]	0.79	0.59	0.69	0.55	[0.35]
15	0.29	0.13	0.44	[0.56]	0.47	0.44	0.38	[0.13]
17	0.19	0.27	[0.37]	0.31	0.57	0.59	0.57	[0.56]
20	0.04	0.00	[0.28]	0.03	0.48	0.50	0.45	[0.20]
25	0.65	0.59	0.77	[0.90]	1.36	1.33	0.81	[0.40]
26	0.35	0.33	[0.54]	0.51	0.77	0.86	0.64	[0.45]
Avg	0.29	0.20	0.45	[0.48]	0.70	0.79	0.61	[0.41]

where p_i^{int} denotes the ground-truth AU intensity of the i -th AU. To compute the w_i using Eq. 3, we treat the intensities of 3, 4, and 5 as the occurrence of AUs. Our WSARL for intensity estimation is named i-WSARL.

To take the correlations between ground-truth and predicted AU intensities into account, we also use a cosine similarity loss formulated as

$$E^{cos} = 1 - \frac{\sum_{i=1}^n p_i^{int} \hat{p}_i^{int}}{\sqrt{\sum_{i=1}^n p_i^{int^2}} \sqrt{\sum_{i=1}^n \hat{p}_i^{int^2}}}, \quad (14)$$

where the second term is the cosine similarity between ground-truth and predicted AU intensities. Thus the complete loss for AU intensity estimation is defined as

$$E = E^{int} + \sum_{i=1}^n E_i^{crf} + \lambda E^{cos}, \quad (15)$$

where the hyperparameter λ is obtained by cross validation in our experiments.

We evaluate AU intensity estimation on two benchmarks, the subset BP4D [28] of FERA 2015 [35], and DISFA [29]. Each frame of both datasets is coded with AU intensities ranging from 0 to 5, in which FERA 2015 is annotated with 5 AUs and DISFA is annotated with 12 AUs. Following the setting of CCNN-IT [36], we perform the experiments using a subject exclusive setting with the same subject partition rule. In particular, the training partition with 21 subjects is used for training and the development partition with 20 subjects is used for testing for FERA 2015, and 18 subjects are used for training and 9 subjects are used for testing for DISFA. Two popular metrics are reported, intra-class correlation (ICC(3,1)) [37] and mean absolute error (MAE).

We compare our method i-WSARL against state-of-the-art methods under the same setting. These methods contain both traditional methods, MRF [38], LT-all [39], and COR-HIT [40], and deep learning based methods, DRML [17], OR-CNN [41], and CCNN-IT [36]. To evaluate methods under the same setting, the results of MRF and LT-all are from [40], and the results of DRML and OR-CNN are from [36].

4.5.1 Evaluation on FERA 2015

Facial AU intensity estimation is a multi-label ordinal classification problem, where many state-of-the-art methods [36], [40], [41] explicitly process the ordinal classification. The ICC and MAE results of different methods on FERA 2015 benchmark is shown in Table 4. It can be seen that our proposed i-WSARL achieves higher ICC and smaller MAE than state-of-the-art works. Although mainly designed for AU detection without considering the ordinal classification, our method performs much better than ordinal methods including OR-CNN, COR-HIT, and CCNN-IT. Our i-WSARL outperforms both traditional methods and deep learning based methods, which demonstrates the effectiveness of our framework.

4.5.2 Evaluation on DISFA

Table 5 shows the AU intensity estimation results on 12 AUs of DISFA. Since DISFA benchmark is annotated with more AUs than FERA 2015, we can observe more comprehensive comparison results. It is seen that our i-WSARL significantly outperforms other deep learning based methods for most of the AUs, especially in terms of the MAE metric. Our framework is superior to all the state-of-the-art AU intensity estimation methods with a simple extension, which indicates the universality of our framework.

4.5.3 Visualization of Attention

We visualize the spatial attention weights $v_i^{(s)}$ of our i-WSARL for 5 AUs of FERA 2015 in Fig. 8. Comparing with the results of AU detection in Fig. 6, we find that the learned spatial attentions of AU intensity estimation occur in a broader facial region and are smoother. This demonstrates that AU intensity estimation requires exploiting more information than AU detection in neighboring regions to estimate the more detailed AU intensities. Moreover, it is also observed that the AU from different expressions of the same person has different attentions. Our proposed framework can adapt diverse expressions and non-rigid AUs for both AU detection and AU intensity estimation.

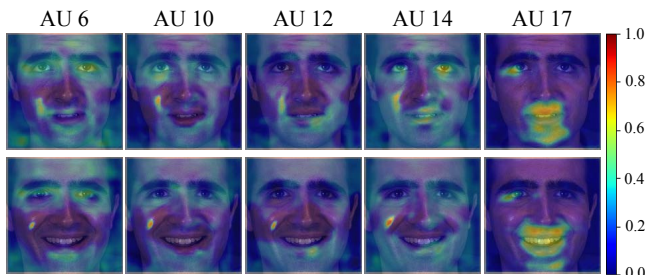


Fig. 8. Visualization of spatial attention weights $v_i^{(s)}$ of our i-WSARL for two example FERA 2015 images. The two images are from a same person with different expressions. Attention weights are visualized with the colors shown in the color bar.

5 CONCLUSION

In this paper, we have proposed an end-to-end weakly-supervised attention and relation learning framework for AU detection. Both channel-wise attention learning and spatial attention learning are used to select and extract AU related features with AU labels only. Moreover, we have proposed the pixel-level relation learning to refine spatial attentions so as to extract more accurate local features. A multi-scale local region learning method is further designed to adapt multi-scale AUs in different locations, which can extract useful features to facilitate the weakly-supervised attention and relation learning.

We have compared our proposed framework against state-of-the-art methods on BP4D and DISFA benchmarks. The AU detection results demonstrate that our framework outperforms the state-of-the-art methods for AU detection. In addition, each component of our framework is indicated to be beneficial for AU detection. Extensive qualitative results demonstrate that our framework can find the ROIs of AUs and capture the relations among AUs adaptively.

We have further applied our framework for AU intensity estimation with a simple extension. Experiments on FERA 2015 and DISFA benchmarks show that our proposed framework can perform well in both AU detection and AU intensity estimation. We believe that the idea of weakly-supervised attention and relation learning is also promising to be applied for other face analysis tasks such as facial expression recognition and face recognition.

ACKNOWLEDGMENTS

This work was supported by the National Natural Science Foundation of China (No. 61503277 and No. 61472245). It was also partially supported by Data Science & Artificial Intelligence Research Centre@NTU (DSAIR), SINGTEL-NTU Cognitive & Artificial Intelligence Joint Lab (SCALE@NTU), and the joint project of Tencent YouTu and Shanghai Jiao Tong University.

REFERENCES

- [1] P. Ekman and E. L. Rosenberg, *What the face reveals: Basic and applied studies of spontaneous expression using the Facial Action Coding System (FACS)*. Oxford University Press, USA, 1997.
- [2] J. Kuen, Z. Wang, and G. Wang, "Recurrent attentional networks for saliency detection," in *IEEE Conference on Computer Vision and Pattern Recognition*. IEEE, 2016, pp. 3668–3677.
- [3] T. Xiao, Y. Xu, K. Yang, J. Zhang, Y. Peng, and Z. Zhang, "The application of two-level attention models in deep convolutional neural network for fine-grained image classification," in *IEEE Conference on Computer Vision and Pattern Recognition*. IEEE, 2015, pp. 842–850.
- [4] Q. You, H. Jin, Z. Wang, C. Fang, and J. Luo, "Image captioning with semantic attention," in *IEEE Conference on Computer Vision and Pattern Recognition*, 2016, pp. 4651–4659.
- [5] W. Li, F. Abtahi, Z. Zhu, and L. Yin, "Eac-net: Deep nets with enhancing and cropping for facial action unit detection," *IEEE Transactions on Pattern Analysis and Machine Intelligence*, 2018.
- [6] W. Li, F. Abtahi, and Z. Zhu, "Action unit detection with region adaptation, multi-labeling learning and optimal temporal fusing," in *IEEE Conference on Computer Vision and Pattern Recognition*. IEEE, 2017, pp. 6766–6775.
- [7] E. Sanchez, G. Tzimiropoulos, and M. Valstar, "Joint action unit localisation and intensity estimation through heatmap regression," in *British Machine Vision Conference*. BMVA Press, 2018.
- [8] Y. Wu and Q. Ji, "Constrained joint cascade regression framework for simultaneous facial action unit recognition and facial landmark detection," in *IEEE Conference on Computer Vision and Pattern Recognition*. IEEE, 2016, pp. 3400–3408.
- [9] A. Newell, K. Yang, and J. Deng, "Stacked hourglass networks for human pose estimation," in *European Conference on Computer Vision*. Springer, 2016, pp. 483–499.
- [10] S. Zheng, S. Jayasumana, B. Romera-Paredes, V. Vineet, Z. Su, D. Du, C. Huang, and P. H. Torr, "Conditional random fields as recurrent neural networks," in *IEEE International Conference on Computer Vision*. IEEE, 2015, pp. 1529–1537.
- [11] S. Hochreiter and J. Schmidhuber, "Long short-term memory," *Neural computation*, vol. 9, no. 8, pp. 1735–1780, 1997.
- [12] X. Zhang and M. H. Mahoor, "Task-dependent multi-task multiple kernel learning for facial action unit detection," *Pattern Recognition*, vol. 51, pp. 187–196, 2016.
- [13] K. Zhao, W.-S. Chu, F. De la Torre, J. F. Cohn, and H. Zhang, "Joint patch and multi-label learning for facial action unit and holistic expression recognition," *IEEE Transactions on Image Processing*, vol. 25, no. 8, pp. 3931–3946, 2016.
- [14] S. Eleftheriadis, O. Rudovic, and M. Pantic, "Multi-conditional latent variable model for joint facial action unit detection," in *IEEE International Conference on Computer Vision*. IEEE, 2015, pp. 3792–3800.
- [15] P. Liu, J. T. Zhou, I. W.-H. Tsang, Z. Meng, S. Han, and Y. Tong, "Feature disentangling machine—a novel approach of feature selection and disentangling in facial expression analysis," in *European Conference on Computer Vision*. Springer, 2014, pp. 151–166.
- [16] Y. Taigman, M. Yang, M. Ranzato, and L. Wolf, "Deepface: Closing the gap to human-level performance in face verification," in *IEEE Conference on Computer Vision and Pattern Recognition*. IEEE, 2014, pp. 1701–1708.
- [17] K. Zhao, W.-S. Chu, and H. Zhang, "Deep region and multi-label learning for facial action unit detection," in *IEEE Conference on Computer Vision and Pattern Recognition*. IEEE, 2016, pp. 3391–3399.
- [18] C. A. Corneanu, M. Madadi, and S. Escalera, "Deep structure inference network for facial action unit recognition," in *European Conference on Computer Vision*. Springer, 2018.

- [19] M. Lin, Q. Chen, and S. Yan, "Network in network," in *International Conference on Learning Representations*, 2014.
- [20] B. Martinez, M. F. Valstar, B. Jiang, and M. Pantic, "Automatic analysis of facial actions: A survey," *IEEE Transactions on Affective Computing*, vol. PP, no. 99, pp. 1–1, 2017.
- [21] A. Krizhevsky, I. Sutskever, and G. E. Hinton, "Imagenet classification with deep convolutional neural networks," in *Advances in neural information processing systems*, 2012, pp. 1097–1105.
- [22] M. Liu, S. Li, S. Shan, and X. Chen, "Au-aware deep networks for facial expression recognition," in *IEEE International Conference and Workshops on Automatic Face and Gesture Recognition*. IEEE, 2013, pp. 1–6.
- [23] S. Ioffe and C. Szegedy, "Batch normalization: Accelerating deep network training by reducing internal covariate shift," in *International Conference on Machine Learning*, 2015, pp. 448–456.
- [24] V. Nair and G. E. Hinton, "Rectified linear units improve restricted boltzmann machines," in *International Conference on Machine Learning*, 2010, pp. 807–814.
- [25] K. He, X. Zhang, S. Ren, and J. Sun, "Deep residual learning for image recognition," in *IEEE Conference on Computer Vision and Pattern Recognition*. IEEE, 2016, pp. 770–778.
- [26] Q. Zhang, Y. N. Wu, and S.-C. Zhu, "Interpretable convolutional neural networks," in *IEEE Conference on Computer Vision and Pattern Recognition*. IEEE, 2018.
- [27] L.-C. Chen, G. Papandreou, I. Kokkinos, K. Murphy, and A. L. Yuille, "Deeplab: Semantic image segmentation with deep convolutional nets, atrous convolution, and fully connected crfs," *IEEE Transactions on Pattern Analysis and Machine Intelligence*, vol. 40, no. 4, pp. 834–848, 2017.
- [28] X. Zhang, L. Yin, J. F. Cohn, S. Canavan, M. Reale, A. Horowitz, P. Liu, and J. M. Girard, "Bp4d-spontaneous: a high-resolution spontaneous 3d dynamic facial expression database," *Image and Vision Computing*, vol. 32, no. 10, pp. 692–706, 2014.
- [29] S. M. Mavadati, M. H. Mahoor, K. Bartlett, P. Trinh, and J. F. Cohn, "Disfa: A spontaneous facial action intensity database," *IEEE Transactions on Affective Computing*, vol. 4, no. 2, pp. 151–160, 2013.
- [30] P. Lucey, J. F. Cohn, T. Kanade, J. Saragih, Z. Ambadar, and I. Matthews, "The extended cohn-kanade dataset (ck+): A complete dataset for action unit and emotion-specified expression," in *IEEE Conference on Computer Vision and Pattern Recognition Workshops*. IEEE, 2010, pp. 94–101.
- [31] Y. Jia, E. Shelhamer, J. Donahue, S. Karayev, J. Long, R. Girshick, S. Guadarrama, and T. Darrell, "Caffe: Convolutional architecture for fast feature embedding," in *ACM International Conference on Multimedia*. ACM, 2014, pp. 675–678.
- [32] R.-E. Fan, K.-W. Chang, C.-J. Hsieh, X.-R. Wang, and C.-J. Lin, "Liblinear: A library for large linear classification," *Journal of Machine Learning Research*, vol. 9, no. Aug, pp. 1871–1874, 2008.
- [33] L. Zhong, Q. Liu, P. Yang, J. Huang, and D. N. Metaxas, "Learning multiscale active facial patches for expression analysis," *IEEE Transactions on Cybernetics*, vol. 45, no. 8, pp. 1499–1510, 2015.
- [34] W.-S. Chu, F. De la Torre, and J. F. Cohn, "Learning spatial and temporal cues for multi-label facial action unit detection," in *IEEE International Conference on Automatic Face & Gesture Recognition*. IEEE, 2017, pp. 25–32.
- [35] M. F. Valstar, T. Almaev, J. M. Girard, G. McKeown, M. Mehu, L. Yin, M. Pantic, and J. F. Cohn, "Fera 2015-second facial expression recognition and analysis challenge," in *IEEE International Conference and Workshops on Automatic Face and Gesture Recognition*, vol. 6. IEEE, 2015, pp. 1–8.
- [36] R. Walecki, O. Rudovic, V. Pavlovic, B. Schuller, and M. Pantic, "Deep structured learning for facial action unit intensity estimation," in *IEEE Conference on Computer Vision and Pattern Recognition*. IEEE, 2017, pp. 5709–5718.
- [37] P. E. Shrout and J. L. Fleiss, "Intraclass correlations: uses in assessing rater reliability," *Psychological Bulletin*, vol. 86, no. 2, p. 420, 1979.
- [38] G. Sandbach, S. Zafeiriou, and M. Pantic, "Markov random field structures for facial action unit intensity estimation," in *IEEE International Conference on Computer Vision Workshops*. IEEE, 2013, pp. 738–745.
- [39] S. Kaltwang, S. Todorovic, and M. Pantic, "Latent trees for estimating intensity of facial action units," in *IEEE Conference on Computer Vision and Pattern Recognition*. IEEE, 2015, pp. 296–304.
- [40] R. Walecki, O. Rudovic, V. Pavlovic, and M. Pantic, "A copula ordinal regression framework for joint estimation of facial action unit intensity," *IEEE Transactions on Affective Computing*, 2017.
- [41] Z. Niu, M. Zhou, L. Wang, X. Gao, and G. Hua, "Ordinal regression with multiple output cnn for age estimation," in *IEEE Conference on Computer Vision and Pattern Recognition*. IEEE, 2016, pp. 4920–4928.